Mater. Sci. Eng. A **725** (2018) 160–170.

Compressive behavior of Cu-Ni alloy foams: Effects of grain size, porosity, pore directionality, and chemical composition

Jenő Gubicza[1,*], Péter Jenei[1], Kyungju Nam[2], Csilla Kádár[1,3], Hyungyung Jo[2] and Heeman Choe[2]

[1]Department of Materials Physics, Eötvös Loránd University, Budapest, P.O.B. 32, H-1518, Hungary

[2]School of Materials Science and Engineering, Kookmin University, 77 Jeongneung-ro, Seongbuk-gu, Seoul 02707, Republic of Korea

[3]Department of Physics of Materials, Charles University, Ke Karlovu 5, CZ12116 Prague 2, Czech Republic

[*]Corresponding author: Tel: + 36-1-372-2876, Fax: +36-1-372-2811,
e-mail: jeno.gubicza@ttk.elte.hu

Abstract

Experiments were conducted to study the compression behavior of Cu-Ni foams prepared using freeze casting. The struts of the foam samples were solid-solutioned with differing Cu/Ni ratios, after which the grain size in the struts was measured using scanning electron microscopy. The compression performance of the samples was studied in both parallel and perpendicular directions to the temperature gradient, and compared with model calculations. It was confirmed that alloying increased the yield strength of the struts. The experimentally determined yield strength and elastic modulus were compared with model calculations, which

revealed that the elastic modulus of the foams was lower than the values calculated from the classical compression and Gibson-Ashby models due to variation in the thickness of the struts. It was also found that the alloying of Cu and Ni improved the mechanical performance of the alloy foams because the absorbed energy for the alloys was considerably higher than that for the pure foams.

Keywords: *Freeze casting; Cu-Ni foams; compression; yield strength; elastic modulus*

1. Introduction

Traditionally, the use of metal foams (mainly closed-celled metal foams) has been limited to structural applications, particularly in the form of sandwich panels that utilize their light weight and excellent bending strength [1-3]. Recently, metal foams with three-dimensional, interconnected open-pore structures have been extensively studied because they hold promise for use in a wide range of engineering applications such as battery electrodes [4], catalysts [5], heat exchangers [6], and filters [7]. For example, the microstructure and compressive strength of Cu foam has been studied for use as an anode in lithium-ion batteries [8, 9], while the processing of Ni foam and its effects on strut morphology were also investigated with a view to utilizing this foam as an anode in dye-sensitized solar cells and polymer-electrolyte-membrane fuel cells [10]. Fe foams have also been proposed, with a major focus on their morphology and the chemical properties of oxide layers grown on the surface, due to their potential use in batteries [11] and water-splitting applications [12]. To satisfy the standard reliability required for the functional devices, the mechanical performance of metallic foams is of great significance even if they are not used in structural applications.

Despite their promise, pure, unalloyed metal foams have a few serious drawbacks.

For example, they may not be suitable for load-bearing structural applications due to their inherent weakness and hardness. In addition to this, their poor corrosion resistance and resultant low reliability can also significantly restrict their functional performance. This is illustrated by freeze-cast open-celled pure Ni foam, which has been proposed for use as the anode gas diffusion layer (GDL) in the membrane electrode assembly within fuel cells due to its superior performance compared to that of conventional carbon-based GDLs, mainly owing to its inherently high electrical conductivity [13]. However, the poor long-term reliability of Ni-foam GDLs in a fuel cell due to their low corrosion resistance in a sulfuric acid environment may prevent their successful practical application [13, 14].

One promising approach to enhancing the reliability and stability of pure metal foams is alloying. In Cu foams, Ni can be an effective alloying element because Cu and Ni form a single-phase solid solution over the entire composition range, improving the mechanical properties of the resulting foam [15]. Furthermore, the melting temperature of Cu-Ni alloys increases almost linearly with the addition of Ni [16]. The advantages of Cu-Ni alloys compared to their pure counterparts have been demonstrated in molten carbonate fuel cells, where the addition of Cu enhanced the reactivity of Ni anodes in alkane hydrogenolysis and dehydrogenation [17]. In addition, Sinfelt et al. [18] demonstrated that the hydrogenolysis activity of Cu-Ni catalysts increased by five orders of magnitude as the proportion of Cu increased from 0 to 60%, suggesting that the use of alloys holds considerable advantages for not only load-bearing but also certain functional applications.

Although alloying has been widely used for bulk alloys using numerous metallic elements to improve their overall strength, the successful synthesis of alloy foams is rare due to the difficulty of foam processing. Therefore, in this study, we applied a powder-based freeze-casting technique to successfully fabricate Cu-Ni alloy foams of varying composition

and analyzed their mechanical performance using compression testing. Their deformation ability was also investigated both parallel and perpendicular to the temperature gradient. To the best of our knowledge, this is the first time the fabrication and the compression behavior of Cu-Ni alloy foams processed by freeze casting has been studied. Yield strength and the elastic modulus were determined experimentally and compared with model calculations, and the influence of variation in strut thickness on compression performance was investigated using theoretical calculations.

2. Experimental material and procedures

2.1. Foam preparation

Commercially available nickel oxide powder (NiO, with an average particle size < 20 nm, Inframat Advanced Materials, USA) and copper oxide powder (CuO, with a particle size of 40-80 nm, Inframat Advanced Materials, USA) were used to produce pure copper, pure nickel, and copper-nickel alloy foams. First, a solution of a 3 wt.% polyvinyl alcohol (PVA) binder with a molecular weight of 89,000-98,000 g mol^{-1} (Sigma-Aldrich, USA) and distilled water was boiled to dissolve the binder. Various ratios of copper and nickel powders were then suspended in the water/binder solution to obtain slurries with nominal Cu content of 100, 70, 50, 30, or 0 wt.%. To improve the stability of the suspension, 0.09 g of Darvan 811, a low-molecular-weight sodium polyacrylate powder dispersant (R.T. Vanderbilt Co., USA), was added [10]. The slurry was then dispersed by stirring for 30 min, followed by sonication for 1 h. This procedure was repeated twice to ensure sufficient particle dispersion. The final slurry was cooled down to a few degrees above the freezing point of water. The slurry was then poured into a cylindrical insulated Teflon mold on a copper rod and then cooled using

liquid nitrogen. The temperature was controlled using a thermocouple and temperature controller. Once complete solidification had been achieved, the frozen green body was removed from the mold and sublimated at -88 °C for 48 h in a freeze-dryer under a residual atmosphere of 0.005 torr to create pores from the sublimated ice. The final green-body foam was then heat-treated by first heating it to a relatively low temperature of 250-300 °C, then maintaining it at that temperature for 2-3 h to remove the binder and reduce the oxide. It was then subsequently sintered under an Ar-5 % H_2 gas mixture at a higher temperature of 800 °C for 6 h, 900 °C for 8 h, or 1000 °C for 3 h for pure Cu, Cu-Ni alloys, or pure Ni foams, respectively. The heating rate was 5 °C/min and the cooling rate was 3 °C/min. The sintered foams containing 100, 70, 50, 30, and 0 wt.% Cu are hereafter referred to as Cu, Cu_7Ni_3, Cu_5Ni_5, Cu_3Ni_7 and Ni foams, respectively.

2.2. Characterization of the microstructure and compression behavior of the foams

The microstructure of the sintered samples was investigated using optical microscopy (PME 3, Olympus, Japan). The phase composition in the struts was investigated using X-ray diffraction (XRD) with a Philips Xpert powder diffractometer and CuKα radiation (wavelength: $\lambda = 0.15418$ nm). The average lattice parameter for the Cu-Ni foams was determined from the position of the diffraction peaks using the Nelson–Riley method [19]. The grain size in the struts of the foams was determined using an FEI Quanta 3D scanning electron microscope (SEM). In order to obtain high-quality SEM images, smooth, distortion-free surfaces were produced using the focused ion beam (FIB) technique in the SEM with Ga ions. For the compression test, rectangular samples were cut from the sintered foams either parallel or perpendicular to the freezing direction using a diamond wheel; in total, five

samples were taken for each Cu-Ni composition and direction combination. The cross-section of the specimens was ~3 × 3 mm^2, while their height was ~5 mm. The compression experiments were carried out using a homemade mechanical testing machine at an initial strain rate of 10^{-3} s^{-1}, and changes in the height of the samples during compression were monitored with an extensometer. The samples were deformed up to an engineering strain of ~0.4.

The density of the samples was determined using the ratio of the mass to the volume of the rectangular specimens. The volume was calculated as the product of the three dimensions of the regular-shaped specimens measured with a micrometer screw gauge.

3. Results

3.1. Microstructure characterization

For each composition of foam, the mean relative density was obtained by averaging the individual values obtained from the five individual samples. The relative densities of the foams are listed in Table 1. For the Cu-containing foams, the relative density varied between ~0.36 and ~0.52, while it was only ~0.25 for the pure Ni foam.

Figs. 1 and 2 present optical micrographs taken of the surfaces lying perpendicular and parallel to the freezing direction (referred to hereafter as the cross and longitudinal sections, respectively). The pore structure is typical of freeze-cast materials, i.e. lamella-like thick struts lying approximately parallel to the freezing direction (Fig. 2). At the same time, the smaller struts lying perpendicular to the freezing direction have no preferred orientation (Fig. 1). Fig. 2 also reveals that the thick struts lying parallel to the freezing direction are

often connected with small perpendicular sticks, as indicated by the white ellipses on the Cu foam image in Fig. 2a. For the pure Ni foam, the struts are thin and have no connecting sticks due to its low relative density.

Fig. 3a presents the XRD patterns for the Cu-Ni alloys. The shift of the peaks to higher angles with increasing Ni content represents a decrease in the lattice parameter. The relationship between the lattice constant, as determined from XRD, and the Ni content of the five alloys is displayed in Fig. 3b. The straight line in this figure represents the theoretical change in the lattice parameter as a function of Ni concentration in Cu-Ni solid solutions. It can be seen that the observed lattice constants are very close to the expected values, suggesting that the struts of all five foam types are a solid solution. This conclusion is also supported by the lack of peaks for other phases in the XRD patterns.

The grain structure in the struts is illustrated in the SEM images in Fig. 4. The thin vertical lines indicate the wavy surfaces caused by the FIB-cutting process, which has been referred to as the “curtaining” effect [20, 21]. The size of the grains ranges between 1 and 5 μm for all samples. Twins were frequently observed inside the grains, some of which were wavy due to the curtaining effect. By considering the twin boundaries to be high-angle grain boundaries, the average grain size for the foams was determined using the linear intercept method (Table 1). The mean grain size varied between 1.0 and 2.8 μm for the Cu-Ni foams. It is evident that, although there was no correlation between the chemical composition and grain size for the studied foams, the pure metals exhibited a smaller grain size than did the alloyed foams. Because the initial powders were nanopowders, grain growth occurred during the sintering process due to the high temperature of consolidation. The evolution of the grain structure in the struts during the sintering process was influenced by many factors, such as sintering time, temperature, and the overall chemical composition of the samples. A higher

sintering temperature and longer sintering time usually lead to larger grains. The homologous temperature for sintering (the temperature normalized by the melting point) was in the range of 0.74−0.79 for the different foams. This slight variation is expected to yield only marginal differences in grain size. At the same time, the sintering times are significantly different and longer consolidation was characteristic of alloy foams, which may have contributed to their larger grain sizes. In addition, during the sintering of the alloy foams, the initial two-phase materials transformed into a single-phase solid solution and this phase transformation may have had an effect on grain growth. However, an in-depth investigation of this effect was beyond the scope of this paper.

3.2. Compression experiments

The mechanical behavior of the foams was investigated by applying uniaxial compression both parallel and perpendicular to the freezing direction. The deformation of the samples during compression testing was recorded on video. As an example, videos showing the deformation parallel and perpendicular to the freezing direction for the Cu_5Ni_5 foam are presented as supplementary materials for this article (see the files “Cu5Ni5_ parallel.flv” and “Cu5Ni5_ perpendicular.flv”, respectively). Fig. 5 presents images from these videos at engineering strains of 0, 0.1, 0.2, 0.3, and 0.4. In the parallel direction, vertical cracks formed in the Cu_5Ni_5 sample even at a strain of 0.1. When applying a strain of 0.2, the specimen started to break vertically into smaller parts. This example of sample failure can be explained by the fracturing of the horizontal sticks connecting the large vertical struts. However, in the perpendicular direction, similar sample deterioration was not observed (Fig. 5) because the struts were oriented perpendicular to the compression direction. The compression behavior of the other foams was similar to that observed for Cu_5Ni_5 foam in both the parallel and perpendicular directions.

Figs. 6a and b display the engineering stress-strain curves for compression parallel and perpendicular to the freezing direction, respectively. The elastic moduli of the samples were obtained from the initial linear section of the stress-strain curves, the results of which are listed in Table 2. The elastic moduli for deformation perpendicular to the freezing direction were smaller than those for compression in the parallel direction. Yield strength was defined as the stress at the end of the linear elastic loading section of the compression curves. The yield strength values parallel and perpendicular to the freezing direction are listed in Table 3. The stress-strain curves recorded in the parallel direction exhibited peak stress at strains below 0.1 (peak stress values are also reported in Table 3). For compression in the parallel direction, the highest yield strength and peak stress were obtained for Cu_5Ni_5 foam, with the lowest measured for Ni foam. The latter observation can be attributed to the very low relative density of Ni foam. For compression in the perpendicular direction, the stress-strain curves did not produce a peak; rather, the stress increased monotonically with increasing strain (Fig. 6b). The energy absorbed during compression up to a strain of 0.4 was calculated as the area under the stress-strain curves for the Cu-Ni foams and presented in Table 4. The highest absorbed energy for the compression experiments, both parallel and perpendicular to the freezing direction, was obtained for the Cu_7Ni_3 and Cu_5Ni_5 samples.

4. Discussion

4.1. Relationship between microstructure and yield strength parallel to freezing direction

All of the parameters characterizing compression behavior, namely the elastic modulus, yield strength, peak stress, and absorbed energy, were influenced by the porosity and geometry of the foams and the grain size and chemical composition of the struts. These features vary

between the different Cu-Ni foams; thus their effects on the mechanical properties of these foams varied as well. The most salient feature of the microstructure of the foams, as determined by the optical micrographs in Figs. 1 and 2, is that the Cu-Ni foams were characterized by thick walls parallel to the freezing direction. Therefore, deformation behavior in the parallel direction can be described by the compression model, for which yield strength is related to relative density using the following equation:

$$\frac{\sigma_Y}{\sigma_{YS}} = C_\sigma^c \rho_{rel}, \quad (1)$$

where σ_Y and σ_{YS} are the yield strength of the foam and the struts, respectively, ρ_{rel} is the relative density, and C_σ^c is a constant that describes the fraction of struts bearing the compression load parallel to the freezing direction. For the studied Cu-Ni foams, C_σ^c must be less than 1 because a proportion of the volume does not bear the load parallel to the freezing direction (e.g., the small sticks connecting the thick struts). Based on previous research (e.g., [22]), a value of 0.5 for C_σ^c was used in Eq. (1).

Because both σ_Y and ρ_{rel} were measured experimentally for the Cu-Ni foams, the yield strength of the struts can be determined from Eq. (1) using $C_\sigma^c = 0.5$. The effect of the chemical composition on strut strength can thus be analyzed. However, it should be noted that grain size also influences the yield strength of the struts, and this differs between the foams. Therefore, the effect of grain size must first be accounted for by calculating the equivalent yield strength for a grain size of 1 μm, which was selected because the pure Cu and Ni foams had similar grain sizes. For the foams with grain sizes that were larger than 1 μm, the equivalent strength (σ_{YS}^*) of the struts was calculated using the Hall-Petch formula:

$$\sigma_{YS}^* = (\sigma_{YS} - \sigma_0) d^{-1/2} + \sigma_0, \quad (2)$$

where σ_0 is the friction stress and *d* is the grain size for the struts (listed in Table 1). For both Cu and Ni, σ_0 is about 20 MPa [23]; this value was also used for the Cu-Ni alloys. Fig. 7 presents equivalent yield strength (σ_{YS}^*) as a function of Ni content, as calculated from Eq. (2). For comparison, previously reported values for the yield strength of bulk Cu and Ni with a grain size of 1 μm are also shown in Fig. 7 [23]; however, similar information was not available for Cu-Ni alloys. For Cu, the calculated equivalent yield strength (205 ± 31 MPa) was in close agreement with the average taken from the literature (~183 MPa). Note that perfect agreement was obtained when $C_\sigma^c = 0.56$. The calculated equivalent yield strength values for the struts in the freeze-casted Cu-Ni foams are listed in Table 5.

For the Ni foam, the equivalent yield strength calculated from the compression model using $C_\sigma^c = 0.5$ was 61 ± 16 MPa, which is much smaller than that obtained from past research (~213 MPa), suggesting that the compression model was not suitable for assessing the compression behavior of Ni foam parallel to the freezing direction. Indeed, Fig. 2e illustrates that the spacing between the struts was very large in Ni foam due to its low relative density (~0.25), and sticks connecting the struts were absent. A previous study also found that, for low relative densities, freeze-cast samples deformed plastically in accordance with the Gibson-Ashby (GA) model or the plastic hinges model parallel to the freezing direction [24]. Therefore, yield strength can be expressed as

$$\frac{\sigma_Y}{\sigma_{YS}} = C_\sigma^{GA} {\rho_{rel}}^{1.5}, \quad (3)$$

where C_σ^{GA} is a constant with a value of about 0.3 [22]. Fig. 7 illustrates good agreement between the equivalent yield strength calculated from Eq. (3) (201 ± 54 MPa) and the data obtained from the literature (~213 MPa [23]). This indicates that, during compression parallel to the freezing direction, macroscopic plastic deformation was initiated by the bending of the

large struts rather than uniaxial compression due to the wide spacing and the lack of connecting sticks. Note that perfect agreement between the calculated and previously reported data was obtained for $C_\sigma^{GA} = 0.28$. The equivalent yield strength of the struts was also calculated for Cu and Cu-Ni foams using Eq. (3), with $C_\sigma^{GA} = 0.28,$ and plotted in Fig. 7. The GA model yielded unrealistically high values for strut strength. In addition, for the pure Cu foam, the experimental strut strength was much smaller than the equivalent yield strength calculated from Eq. (3). Therefore, it can be concluded that the GA model does not accurately describe plastic flow parallel to the freezing direction in Cu and Cu-Ni foam struts. It is also worth mentioning that Scotti and Dunand [24] suggested that the relative density corresponding to the transition between the compression and the GA models was 0.4−0.5. For the freeze-cast Cu-Ni foams in this study, this relative density limit might be smaller than 0.4; Figs. 1 and 2 show that the Cu-Ni foams with relative densities between 0.36 and 0.52 exhibited similar structures to the Cu foam, which was in accordance with the compression model. Therefore, the relative density limit corresponding to the transition between the compression and the GA models might be between 0.25 and 0.36.

Because the structure of the Cu-Ni foams was similar to that of the Cu foam (Figs. 1 and 2), the equivalent yield strength for the Cu-Ni alloys was determined from Eq. (1) using $C_\sigma^c = 0.5$ and plotted in Fig. 7. It can be seen that, while the equivalent yield strength for the pure Cu and Ni foams was about 200 MPa, the corresponding values for the Cu-Ni alloy foams were higher. The largest equivalent yield strength was obtained for Cu_5Ni_5 (364 ± 71 MPa), which suggests that the higher the degree of alloying, the higher the yield strength of the struts. It is noted here that all of the foams were solid solutions, as proven by the XRD measurements (see Fig. 3 and Section 3.1). Therefore, the alloying element content agrees with the nominal composition of the foams. As mentioned earlier, grain size also had an

influence on the strength of the struts, in accordance with the Hall-Petch equation.

4.2. Correlation between the pore structure and the elastic modulus measured parallel to the freezing direction

In accordance with the results obtained for yield strength, the elastic moduli of the Cu and the Cu-Ni foams for deformation parallel to the freezing direction were calculated from the compression model using the following equation:

$$\frac{E}{E_S} = C_E^c \rho_{rel}, \quad (4)$$

where E and E_S are the moduli of the foams and the bulk material in the struts, respectively, and C_E^c is a constant that describes the fraction of struts bearing the compression load parallel to the freezing direction. For this calculation, the value for E_S was taken from the literature [25]. Assuming the same value of C_E^c for the Cu and the Cu-Ni foams, the smallest difference between the measured and calculated elastic moduli was obtained when C_E^c = 0.11. Fig. 8 presents the measured and calculated moduli for compression parallel to the freezing direction. This smaller value of C_E^c = 0.11 was significantly smaller than the constant C_σ^{GA} (~0.5) used for the calculation of yield strength. At the same time, C_σ^c and C_E^c must be equal in the classical compression model. The small value for C_E^c indicates that the classical compression model was unsuitable for the studied foams and the measured elastic moduli were smaller than the values estimated from Eq. (2) using the classical value of ~0.5 for C_E^c.

As described earlier, the yield strength of Ni foam followed the GA model, thus the elastic modulus for this material was calculated from the elastic buckling model:

$$\frac{E}{E_S} = C_E^{GA}{\rho_{rel}}^2, \quad (5)$$

where C_E^{GA} is a constant. The agreement between the measured and calculated elastic moduli for Ni foam was obtained for C_E^{GA} = 0.16 (see Fig. 8). This is smaller than previously published values for the GA model ($C_E^{GA} \approx 0.3$), which also indicates that the observed modulus is lower than that predicted by the classical model.

The lower values for the measured elastic moduli compared to the values predicted using the classical models can be explained by variation in the structure of the struts parallel to the freezing direction. Stress is higher in thinner sections of the struts, which can lead to local plastic yielding, while the thicker sections only deform elastically; this microplastic deformation reduces the measured elastic modulus. In addition, the variation in thickness in the struts along the freezing direction can cause a lower apparent elastic modulus even if the deformation remains elastic in the thinner sections of the struts (this variation in thickness can be seen in Fig. 2). This effect can be understood when the elastic modulus of a single strut composed of thicker and thinner sections is calculated (Fig. 9a). Under a loading parallel to the strut, the apparent stress is calculated as the ratio of the force (F) and the cross-section of the walls (A) if a uniform wall thickness is assumed. The latter quantity can be calculated as

$$A = \frac{A_1 l_1 + A_2 l_2}{l_1 + l_2}, \quad (6)$$

where A_1 and A_2 are the cross-sections while l_1 and l_2 are the lengths of the two strut sections (Fig. 9a). The apparent strain of the wall (ε) can be calculated as

$$\varepsilon = \frac{\varepsilon_1 l_1 + \varepsilon_2 l_2}{l_1 + l_2}, \quad (7)$$

where ε_1 and ε_2 are the local strain in the two strut sections, which can be expressed as

$$\varepsilon_1 = \frac{F}{EA_1} \text{ and } \varepsilon_2 = \frac{F}{EA_2}, \quad (8)$$

where *E* is the real elastic modulus of the struts. The apparent elastic modulus can be calculated from the following formula:

$$E_a = \frac{F}{\varepsilon A}. \quad (9)$$

From Eqs. (6-9), the apparent elastic modulus can be expressed as

$$E_a = E\frac{l_r^2+1+2l_r}{l_r^2+1+(A_r+A_r^{-1})l_r}, \quad (10)$$

where l_r is the ratio of the lengths of the two strut sections ($l_r = \frac{l_1}{l_2}$; Fig. 9a) and A_r is the ratio of the areas of the two strut sections ($A_r = \frac{A_1}{A_2}$; Fig. 9a). Because $A_r + A_r^{-1}$ is larger than 2 for all A_r values (Fig. 9b), the apparent elastic modulus is smaller than the real elastic modulus *E*. Therefore, for a strut that varies in thickness, the measured elastic modulus is always lower than the modulus of the strut material. For example, if $l_1 = l_2$ and $A_1 = 6A_2$, the apparent elastic modulus is half of the real value. This effect probably contributed to the relatively small observed values for the elastic moduli of the Cu-Ni foams in the present study. However, it should be noted that the horizontal sticks connecting the vertical struts were able to mitigate this effect.

Figs. 10a and b present two struts that vary in thickness along their length and that are connected with horizontal sticks in two different ways. In Fig. 10a, it is evident that the thin sections of the struts are connected by the sticks, while in Fig. 10b, a thin section is connected to a thick section in the neighboring strut. The sticks have little effect on the elastic modulus in the former case, while the latter case can significantly lower the modulus degradation

caused by strut inhomogeneity. This is because the horizontal sticks in the latter case produce similar local strain in the thick and thin sections of the struts. It should be noted that heterogeneity in the thickness of the struts also has an effect on macroscopic yield strength, which is defined as the stress required for the plastic deformation of the entire sample and is determined by the thickest sections of the struts. Thus, macroscopic yield strength increases with greater variation in strut thickness due to the formation of thicker strut sections. It can be concluded that variation in thickness within individual struts likely led to the considerable difference between the values of C_{σ}^{c} and C_{E}^{c}.

4.3. Influence of porosity and strut morphology on elastic modulus measured perpendicular to freezing direction

Compression behavior perpendicular to the freezing direction can be described by the GA model because long struts lying parallel to the freezing direction bend under a compression load perpendicular to the freezing direction [22]. Fig. 11 displays the elastic moduli of the Cu-Ni foams measured perpendicular to the freezing direction. These values were influenced by the moduli of the struts and the relative density, as described in Eq. (5). In the original GA model, C_{E}^{GA} is a constant equal to unity [26]. However, previous experimental studies have shown that C_{E}^{GA} depends on foam geometry and is typically between 0.3 and 0.5 [27]. For the Cu-Ni foams in the present study, the experimentally measured elastic moduli and the values calculated from the GA model were in close agreement if C_{E}^{GA}= 0.08 (Fig. 11). This relatively small value of C_{E}^{GA} can be attributed to inhomogeneity in the freeze-cast microstructure. This effect is similar to the relatively low C_{E}^{c} for compression applied parallel to the freezing direction (Section 4.2), which was caused by the variation in thickness

within the struts.

For compression applied perpendicular to the freezing direction, C_E^{GA} decreases with increasing variation in the thickness of different struts. This effect can be illustrated using the simple model depicted in Fig. 12a, where two struts with different thicknesses are shown (for simplicity, variation in strut thickness along the freezing direction is not shown). These struts are connected with the neighboring walls by small sticks. The deflection of the struts between the sticks causes the contraction of the foam perpendicular to the freezing direction. The deflection of a strut with thickness *b* loaded by force *F* is proportional to *F* and inversely proportional to the cube of *b*. Therefore, the total contraction resulting from two struts with thicknesses of b_1 and b_2 can be expressed as

$$\Delta l = B\sigma\left(\frac{1}{b_1^3}+\frac{1}{b_2^3}\right), \tag{11}$$

where σ is the applied stress. Factor *B* depends on the elastic modulus of the struts, the surface area perpendicular to the load, the thickness of the struts perpendicular to the schematic in Fig. 12a, the number of horizontal sticks, and the spacing between the sticks. The engineering strain can be obtained as the ratio of Δl to the horizontal thickness of the sample (*l*). The effective elastic modulus can thus be calculated as the ratio between the stress and the strain. For different strut thicknesses, i.e., for different b_1 and b_2 values, the measured elastic modulus can be calculated as

$$E_{inhom} = \frac{l}{B}\left(\frac{1}{b_1^3}+\frac{1}{b_2^3}\right)^{-1}. \tag{12}$$

For uniform strut thicknesses, the elastic modulus is given by

$$E_{uniform} = \frac{l}{B}\left(\frac{2}{b^3}\right)^{-1}, \tag{13}$$

where $b = \frac{b_1+b_2}{2}$ because strut volume is considered to be constant. The relative change in the modulus due to variation in strut thickness can be written as

$$\frac{E_{inhom}}{E_{uniform}} = 2\left[\left(\frac{b_1}{b}\right)^{-3} + \left(2 - \frac{b_1}{b}\right)^{-3}\right]^{-1}. \quad (14)$$

The function in Eq. (14) where $\frac{b_1}{b}$ varies between 0 and 2 is plotted in Fig. 12b. A uniform strut thickness corresponds to $\frac{b_1}{b}$ = 1. For $b_1 \neq b_2$, $\frac{E_{inhom}}{E_{uniform}}$ is smaller than 1, i.e., variation in strut thickness leads to a smaller modulus than for uniform struts. In the GA model, the smaller observed modulus caused by strut thickness variation can be taken into account by lowering C_E^{GA}. It should be noted that, although the elastic deformation of the small sticks between the large struts is likely to contribute to elastic deformation, this effect is marginal when compared to differences caused by the variation in thickness between large struts.

4.4. Effect of microstructure on yield strength measured perpendicular to freezing direction

Fig. 13 presents the yield strength of the Cu-Ni foams measured perpendicular to the freezing direction as a function of Ni content. In addition, yield strength was calculated from the GA plastic hinges model using Eq. (3) and plotted in Fig. 13. For the yield strength of the struts (σ_{YS}) in Eq. (3), the values determined for the parallel direction were used (Section 4.1). The closest agreement between the measured and calculated values was obtained when C_σ^{GA}= 0.14. It should be noted that C_σ^{GA} is influenced by foam structure, so it may differ for the various Cu-Ni foams. For instance, for the pure Cu foam, close agreement between the measured and calculated strength was achieved with values of C_σ^{GA} higher than 0.14. In the GA plastic hinges model, it is assumed that plastic deformation is restricted to the junctions

of the struts while the other sections of the struts remain rigid. At the same time, the internal stress in the bending struts may cause plasticity outside of the junctions. Therefore, depending on the foam microstructure, the relative contributions of the junctions and the strut interiors to plasticity may vary, resulting in different C_{σ}^{GA} values, as suggested by Fig. 13.

4.5. Influence of alloying on the energy absorbed during compression

Fig. 14 shows that the energy absorbed by the foams during compression to a strain of 0.4 is the highest for the Cu_7Ni_3 and Cu_5Ni_5 alloys, which can be explained by the high flow stress, as presented in Fig. 6. For the Cu_7Ni_3 alloy, high flow stress was caused mainly by the large relative density (Table 1). For the Cu_5Ni_5 alloy, although the relative density was not particularly high, the yield strength of the struts was very high due to the alloying effect (Table 5), which yielded high flow stress and consequently large absorbed energy. Absorbed energy in relation to Ni content exhibited a similar trend for compression perpendicular to and deformation parallel to the freezing direction (Fig. 14), with alloying significantly increasing the energy absorbed in the Cu and Ni foams. Solid-solution hardening in the struts of the foams yielded not only higher yield strength but also greater strain hardening during deformation due to the higher multiplication rate and the hindered annihilation of dislocations, which confirms that the alloying of Cu and Ni foams is highly beneficial for structural applications.

5. Conclusions

Cu-Ni foams that differed in Ni content were processed using freeze casting. Their

compression behavior was studied parallel and perpendicular to the freezing direction up to an engineering strain of 0.4. The following conclusions can be drawn from the results.

1. For compression parallel to the freezing direction, the Cu-Ni foams behaved in accordance with the compression model, except for the pure Ni foam. Ni foam had a very low relative density (~0.25), thus the very thin struts may have buckled under the vertical load. Therefore, the GA model is more appropriate for the calculation of yield strength and the elastic modulus for the compression of Ni foam parallel to the freezing direction. The yield strength of the struts was higher for the alloys than for the pure metal foams.

2. In the classical compression model, C_E^c and C_σ^c, which are used for the calculation of the elastic modulus and yield strength, respectively, have the same value. Our calculations revealed that variation in the thickness of the struts resulted in a C_E^c that was significantly smaller than C_σ^c. This difference was also observed experimentally for the studied Cu-Ni foams.

3. The behavior of the Cu-Ni foam perpendicular to the freezing direction was successfully described by the GA model, and the theoretical calculations also supported the trend that the measured elastic modulus decreased with increasing variation in strut thickness. Therefore, C_E^{GA}, which was used to calculate elastic moduli, was smaller than the value obtained for the classical GA model.

4. The absorbed energy measured during compression up to a strain of 0.4 was higher for the alloys than for the pure foams, irrespective of the direction of compression. Therefore, we conclude that alloying improves the compression performance of Cu and Ni foams processed using freeze casting.

Acknowledgments

The authors are indebted to National Research, Development, and Innovation Office Grant nos. K-109021 and PD-121049 for financial support. Choe also acknowledges support from the National Research Foundation (NRF) of Korea (2009-0093814, 2014R1A2A1A11052513). This paper was supported by the János Bolyai Research Scholarship of the Hungarian Academy of Sciences. The authors are grateful for the financial support of the Czech Science Foundation under the contract 15-10821S.

References

[1] L.-P. Lefebvre, J. Banhart, D.C. Dunand, Porous metals and metallic foam: Current status and recent developments, Adv. Eng. Mater. 10 (2008) 775-787.

[2] J. Banhart, Manufacture, characterization, and application of cellular metals and metal foams, Prog. Mater. Sci. 46 (2001) 559-632.

[3] G.J. Davies, S. Zhen, Metallic foams: Their production, properties and applications, J. Mater. Sci. 18 (1983) 1899-1911.

[4] P. Zhao, H. Zhang, H. Zhou, B. Yi, Nickel foam and carbon felt applications for sodium polysulfide/bromine redox flow battery electrodes, Electrochim. Acta 51 (2005) 1091-1098.

[5] R. Horn, K.A. Williams, N.J. Degenstein, A.Bitsch-Larsen, D.D. Nogare, S.A. Tupy, L.D. Schmidt, Methane catalytic partial oxidation on autothermal Rh and Pt foam catalysts: Oxidation and reforming zones, transport effects, and approach to thermodynamic equilibrium, J. Catal. 249 (2007) 380-393.

[6] S. Mellouli, H. Dhaou, F. Askri, A. Jemni, S.B. Nasrallah, Hydrogen storage in metal hydride tanks equipped with metal foam heat exchanger, Int. J. Hydrog. Energy 24 (2009) 9393-9401.

[7] M.S.A. Heikkinen, N.H. Harley, Experimental investigation of sintered porous metal foam, J. Aerosol Sci. 31 (2000) 721-738.

[8] J.H. Um, H. Park, Y.-H. Cho, M.P.B. Glazer, D.C. Dunand, H. Choe, Y.-E. Sung, 3D interconnected SnO2-coated Cu foam as a high-performance anode for lithium-ion battery applications, RSC Adv. 4 (2014) 58059-58063.

[9] J.H. Um, M. Choi, H. Park, Y.-H. Cho, D. C. Dunand, H. Choe, Y. Sung, 3D macroporous electrode and high-performance in lithium-ion batteries using SnO2 coated on Cu foam, Sci. Rep. 6 (2016) 18626(1-9).

[10] H. Jo, M. Kim, H. Choi, Y. Sung, H. Choe, D. C. Dunand, Morphological study of directionally freeze-cast nickel foams, Metall. Mater. Trans. E 3 (2016) 46-54.

[11] H. Park, Y. Noh, H. Choi, K. Hong, K. Kwon, H.Choe, Processing, microstructure, and oxidation behavior of iron foams, Metall. Mater. Trans. A 47 (2016) 4760-4766.

[12] J. Kang, Y. Noh, J. Kim, H. Choi, T. Jeon, D. Ahn, J. Kim, S. Yu, H. Park, J. Yum, W. Choi, D. C. Dunand, H. Choe, Y. Sung, Iron oxide photoelectrode with multidimensional architecture for highly efficient photoelectrochemical water splitting, Angew. Chem. 129 (2017) 6683-6688.

[13] F. Bidault, D.J.L. Brett, P.H. Middleton, N. Abson, N.P. Brandon, A new application for nickel foam in alkaline fuel cell, Int. J. Hydrogen Energy 34 (2009) 6799-6808.

[14] F.-P. Ting, C.-W. Hsieh, W.-H. Weng, J.-C. Lin, Effect of operational parameters on the performance of PEMFC assembled with Au-coated Ni-foam, Int. J. Hydrog. Energy 37 (2012) 13696-13703.

[15] I. Baskaran, T.S.N.S. Narayanan, A. Stephen, Pulsed electrodeposition of nanocrystalline Cu–Ni alloy films and evaluation of their characteristic properties, Mater. Lett. 60 (2006) 1990-1995.

[16] L. Yu, Y. Jiang, Y. He, C.T. Liu, The corrosion behavior of sintering micro-porous Ni–Cu alloy in hydrofluoric acid solution, J. Alloys Compd. 37 (2012) 13696-13703.

[17] E.R. Hwang, J.W. Park, Y.D. Kim, S.J. Kim, S.G. Kang, Effect of alloying elements on the copper-base anode for molten carbonate fuel cells, J. Power Sources 69 (1997) 55-60.

[18] J.H. Sinfelt, J.L. Carter, D.J.C. Yates, Catalytic hydrogenolysis and dehydrogenation over copper-nickel alloys, J. Catal. 24 (1972) 283-296.

[19] J. Nelson, D. Riley, An experimental investigation of extrapolation methods in the derivation of accurate until-cell dimensions of crystals, Proc. Phys. Soc. 57 (1945) 160–177.

[20] L.A. Giannuzzi, F.A. Stevie, (eds.), Introduction to Focused Ion Beams: Instrumentation, Theory, Techniques and Practice, Springer, New York, 2005.

[21] T. Ishitani, K. Umemura, T. Ohnishi, T. Yaguchi, T. Kamino, Improvements in performance of focused ion beam cross-sectioning: aspects of ion–sample interaction, J. Electron. Microsc. 53 (2004) 443-449.

[22] H. Park, M. Choi, H. Choea, D.C. Dunand, Microstructure and compressive behavior of ice-templated copper foams with directional, lamellar pores, Mater. Sci. Eng. A 679 (2017) 435–445.

[23] J. Gubicza, Defect Structure and Properties of Nanomaterials, second and extended ed., Woodhead Publishing, Duxford, UK, 2017.

[24] K.L. Scotti, D.C. Dunand, Freeze Casting – A Review of Processing, Microstructure and Properties via the Open Data Repository, arXiv preprint (2017) arXiv:1710.00037

[25] E. Iguchi, K. Udagawa, Analysis of Young's modulus in the polycrystalline Cu-Ni alloy with the theory for Nordheim's rule, J. Phys. F: Met. Phys. 5 (1975) 214-226.

[26] L. J. Gibson, M. F. Ashby, Cellular Solids: Structures and Properties, Cambridge

University Press, NY 1997.

[27] N.A. Fleck, An overview of the mechanical properties of foams and periodic lattice materials, in: Proceedings of Symposium on Cellular Metals and Polymers. Fuerth, Germany, 2004, pp. 1-4.

Figure and table captions

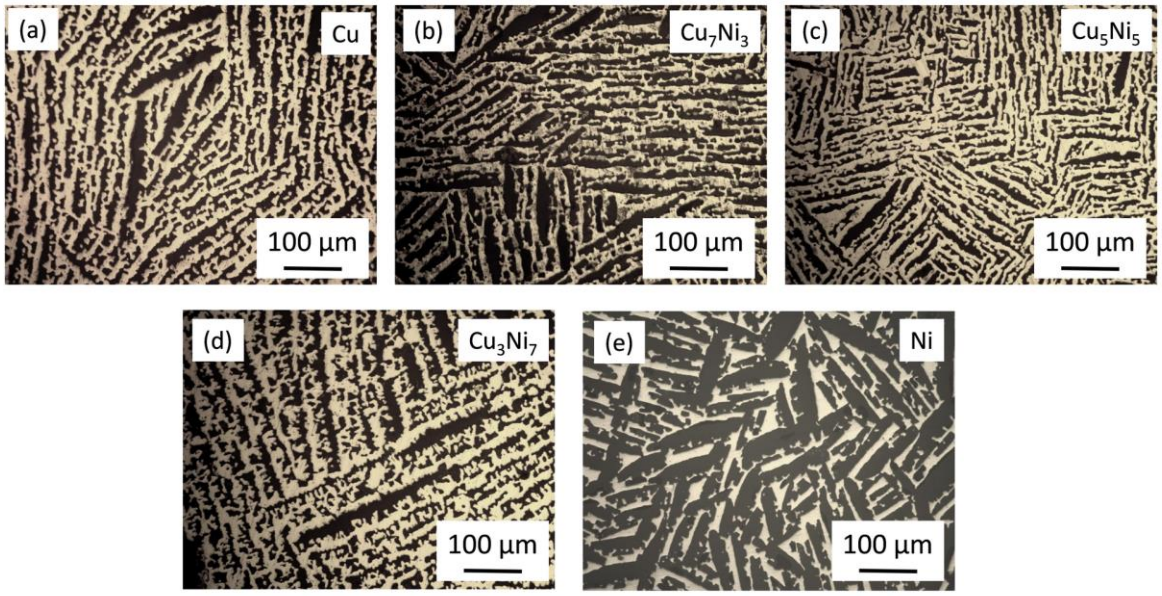

Fig. 1: Optical micrographs of the surface lying perpendicular to the freezing direction.

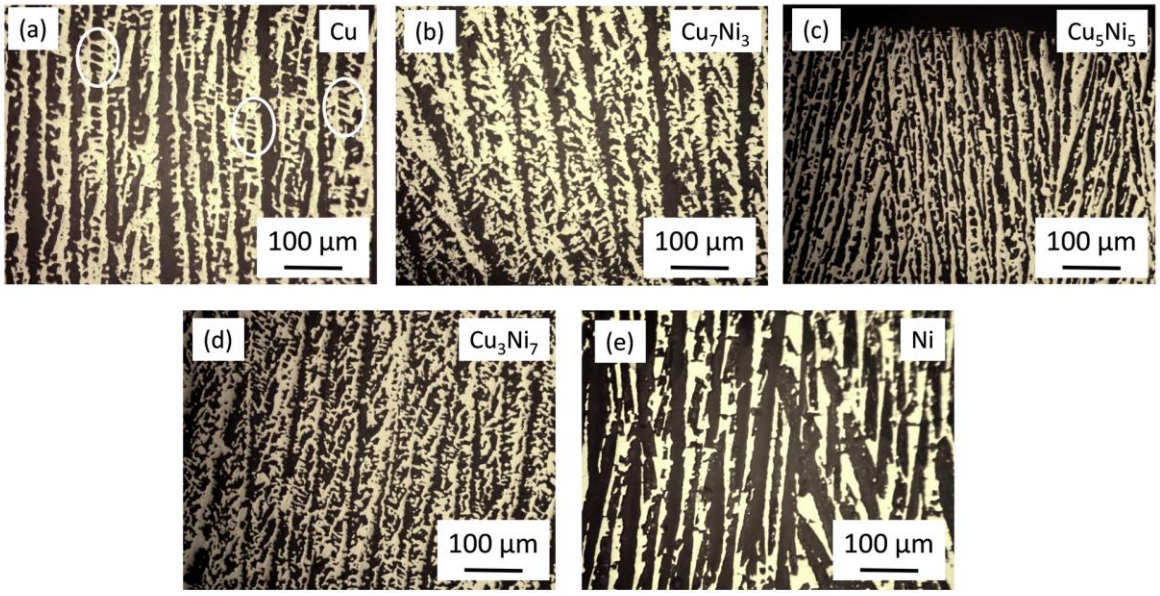

Fig. 2: Optical micrographs of the surface lying parallel to the freezing direction. The white ellipses in (a) show thick struts lying parallel to the freezing direction connected with perpendicular small sticks.

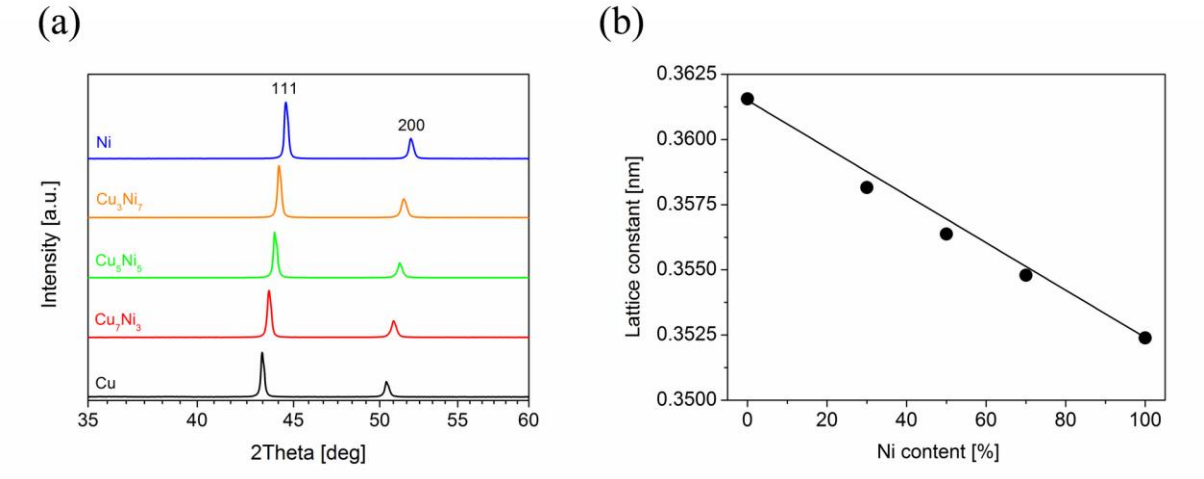

Fig. 3: (a) XRD patterns for the different Cu-Ni alloys. (b) The lattice constant determined by XRD as a function of the Ni content of the foams.

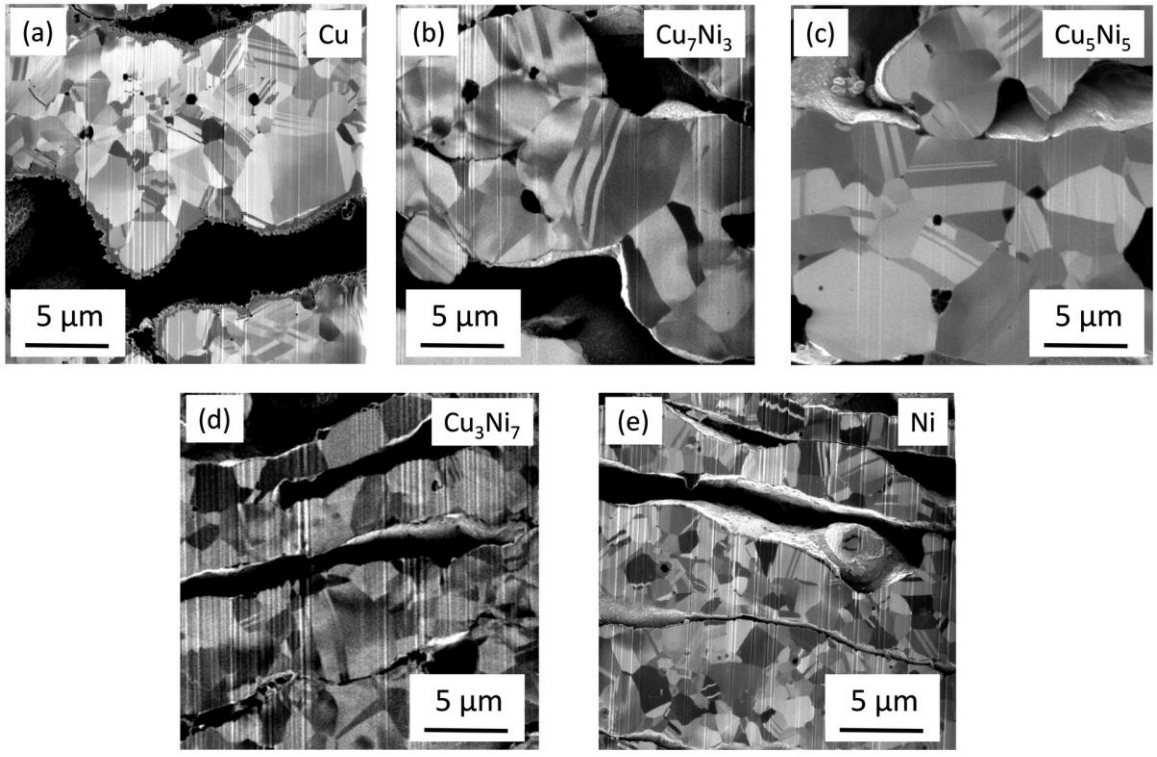

Fig. 4: SEM images showing the grain structure of the foam struts.

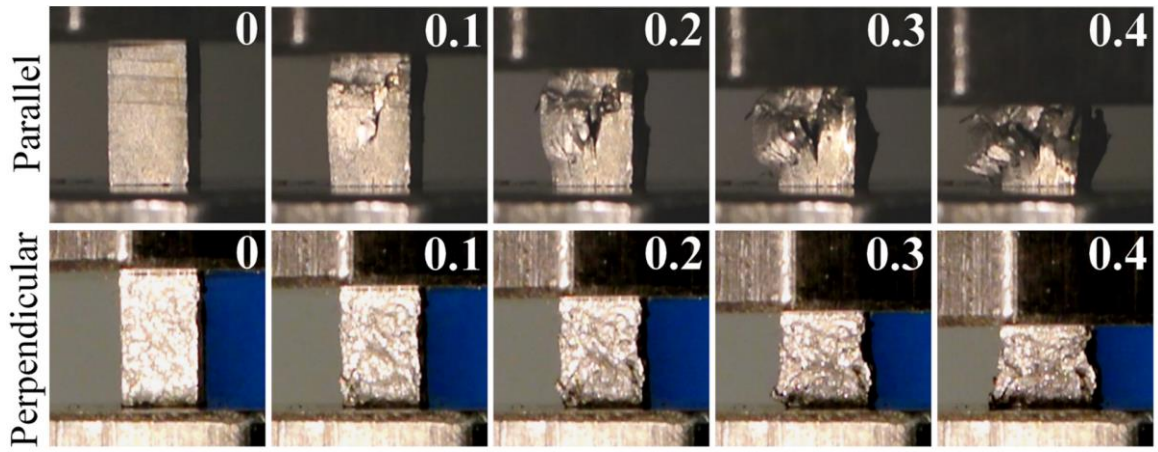

Fig. 5: Images showing the deformation for the Cu_5Ni_5 foam at engineering strains of 0, 0.1, 0.2, 0.3, and 0.4 parallel and perpendicular to the freezing direction.

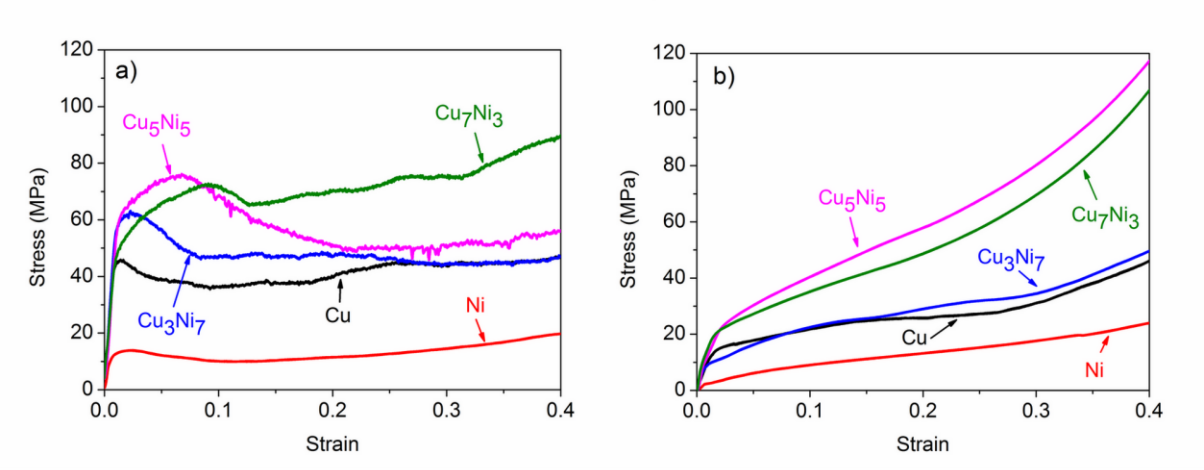

Fig. 6: The engineering stress-strain curves for compression testing parallel and perpendicular to the freezing direction.

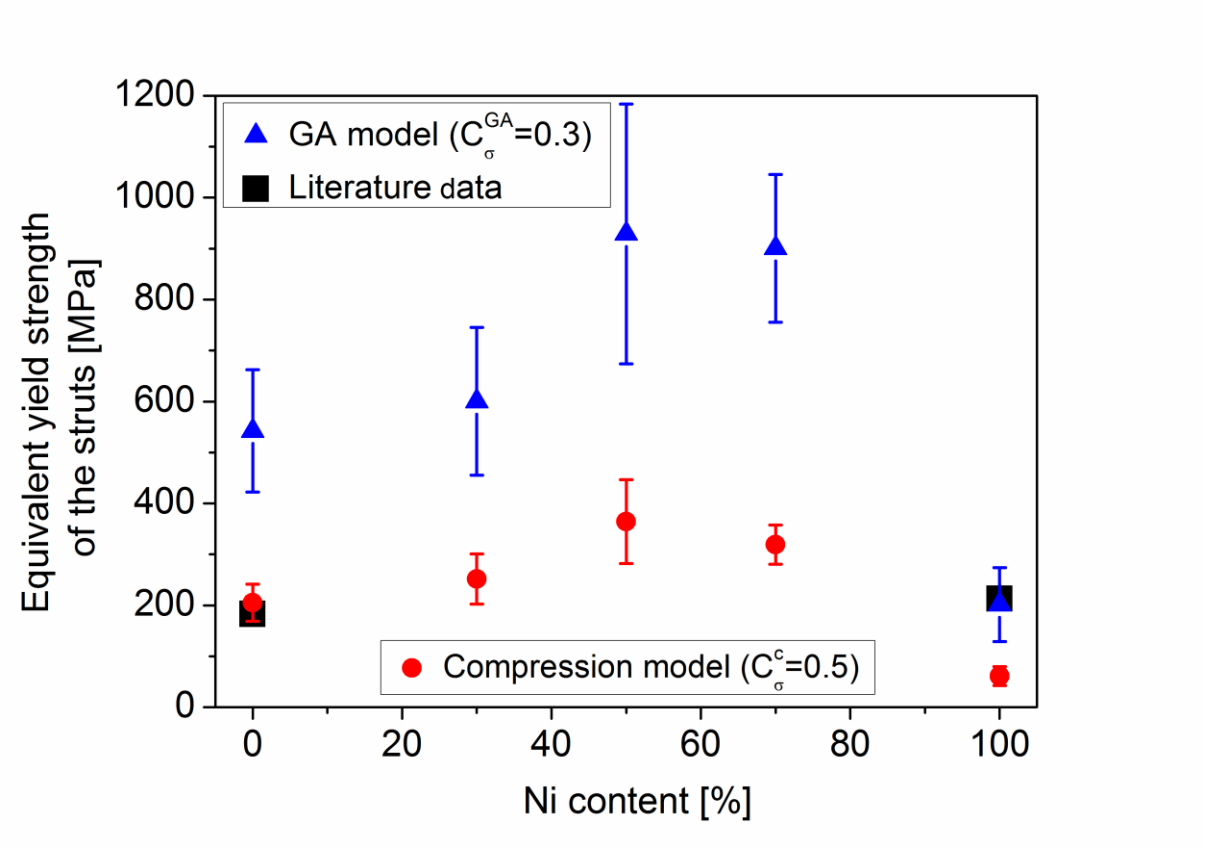

Fig. 7: The calculated equivalent yield strength of the struts for the freeze-casted Cu-Ni foams with a grain size of 1 μm as a function of Ni content. GA model: Gibson-Ashby model.

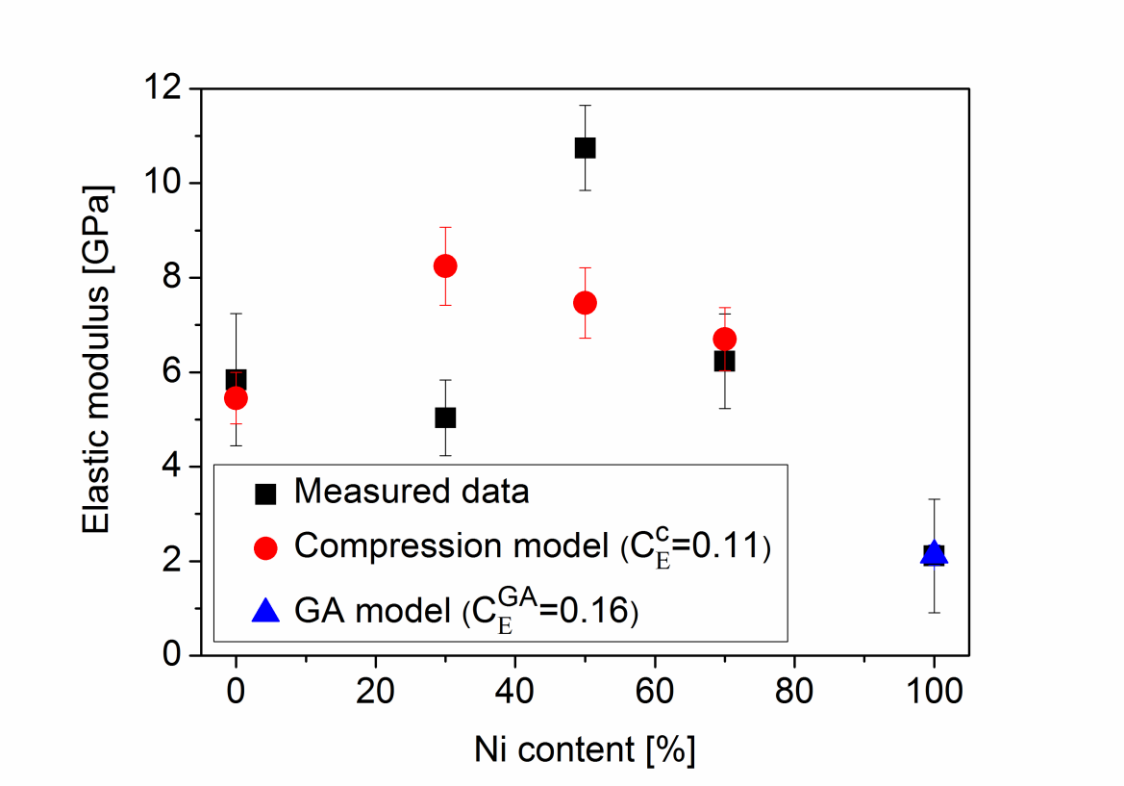

Fig. 8: The elastic moduli of the Cu-Ni foams measured by compression parallel to the freezing direction obtained by model calculations as a function of Ni content. GA model: Gibson-Ashby model.

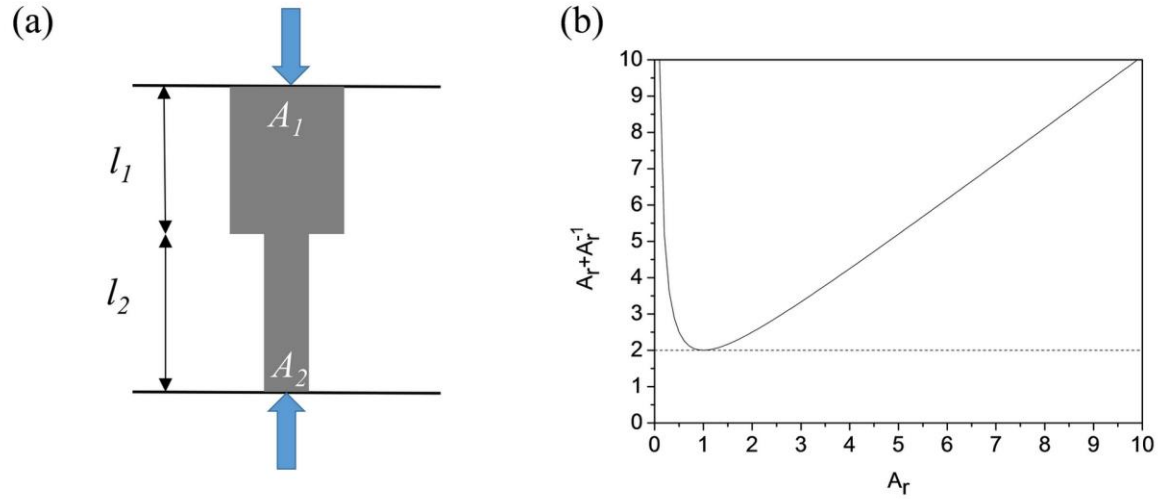

Fig. 9: (a) A single strut consisting of thick and thin sections. (b) $A_r + A_r^{-1}$ as a function of A_r, where $A_r = \frac{A_1}{A_2}$ (see a).

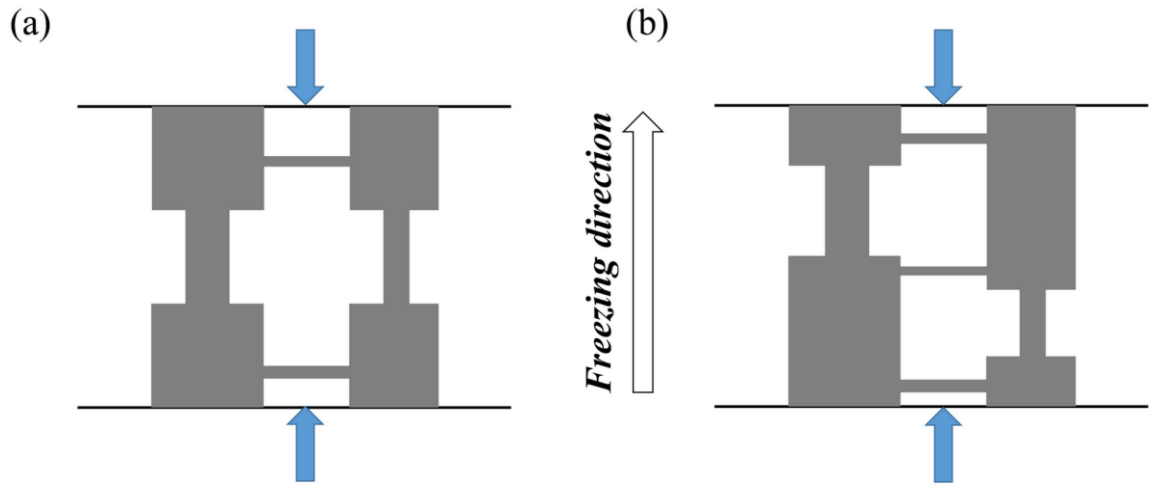

Fig. 10: Schematic of two struts that vary in thickness connected with horizontal sticks in two different ways: (a) the thin sections of the struts are connected by sticks and (b) a thin section is connected to a thick section in the neighboring strut.

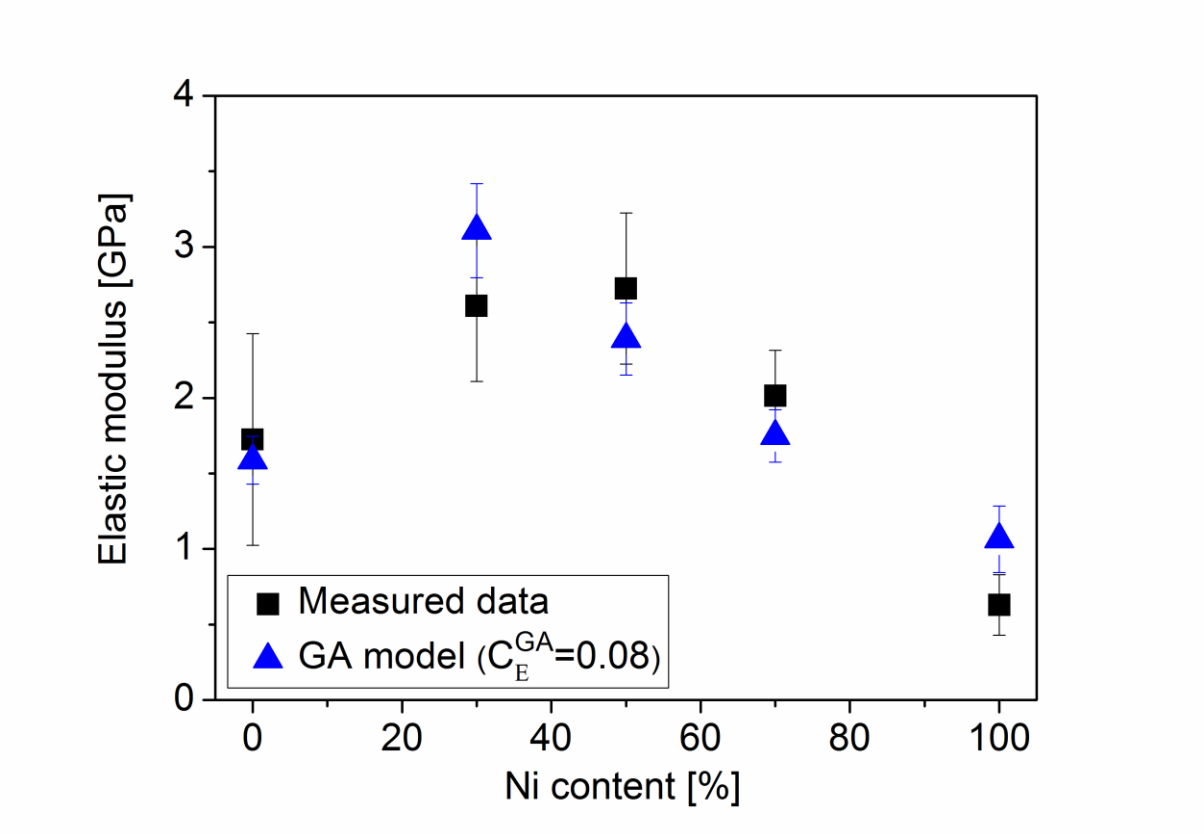

Fig. 11: The elastic moduli for the Cu-Ni foams measured by compression perpendicular to

the freezing direction and obtained by model calculations as a function of Ni content. GA model: Gibson-Ashby model.

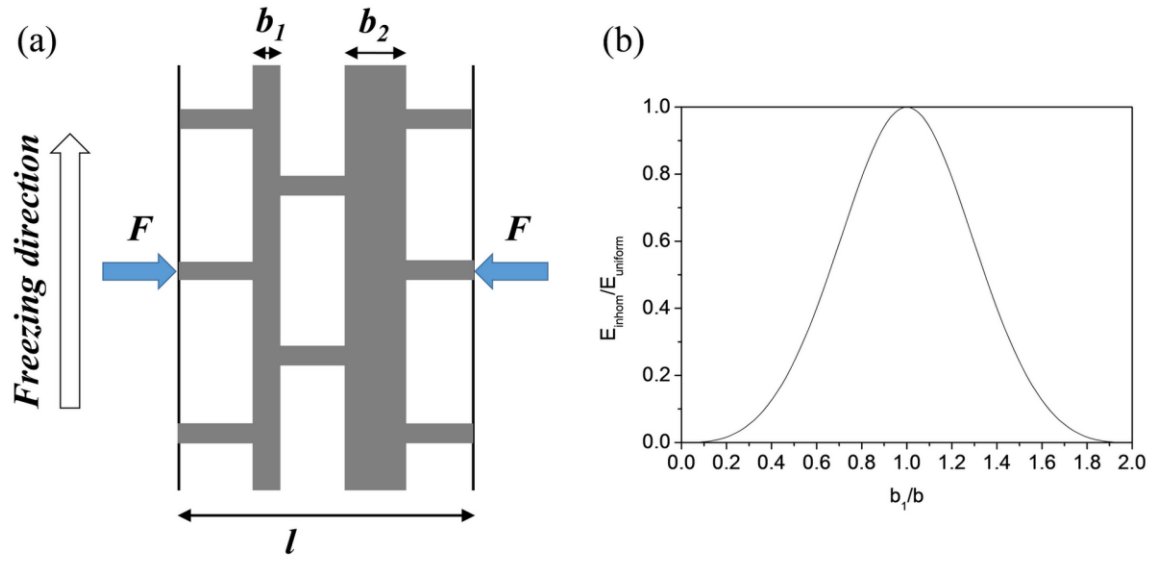

Fig. 12: (a) Schematic of two struts with different thicknesses loaded perpendicular to the freezing direction. (b) $\frac{E_{inhom}}{E_{uniform}}$ as a function of $\frac{b_1}{b}$ according to Eq. (14).

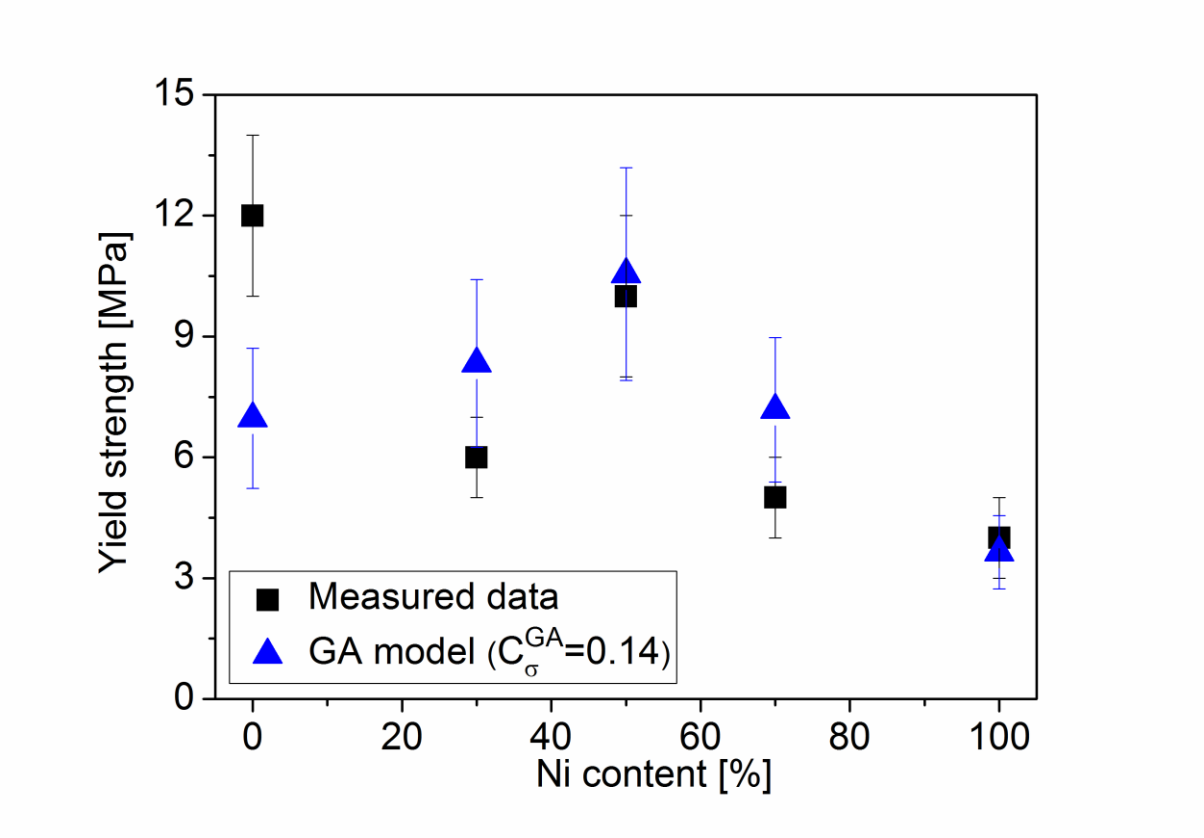

Fig. 13: The yield strength for the Cu-Ni foams measured by compression perpendicular to the freezing direction and obtained by model calculations as a function of Ni content. GA model: Gibson-Ashby model.

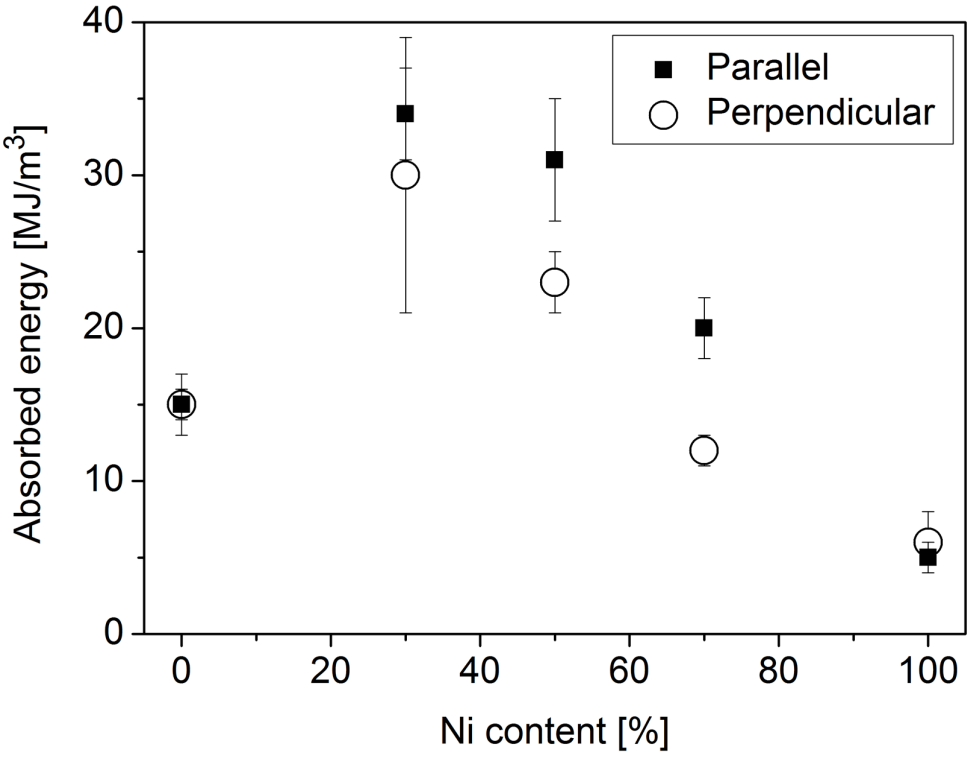

Fig. 14: The energy absorbed by the foams as a function of Ni content during compression at a strain of 0.4 for the freeze-casted Cu-Ni foams.

Table 1: The relative density and the average grain size for the freeze-casted Cu-Ni foams.

Composition	Relative Density	Grain Size [µm]
Cu	0.40 ± 0.01	1.1
Cu_7Ni_3	0.52 ± 0.03	2.8
Cu_5Ni_5	0.44 ± 0.02	2.3
Cu_3Ni_7	0.36 ± 0.01	1.9
Ni	0.25 ± 0.03	1.0

Table 2: The elastic moduli determined by compression testing parallel and perpendicular to the freezing direction for the freeze-casted Cu-Ni foams.

Composition	Elastic Modulus [GPa]	
	Parallel	Perpendicular
Cu	5.8 ± 1.4	1.7 ± 0.7
Cu_7Ni_3	5.0 ± 0.8	2.6 ± 0.5
Cu_5Ni_5	10.7 ± 0.9	2.7 ± 0.5
Cu_3Ni_7	6.2 ± 1.0	2.0 ± 0.3
Ni	2.1 ± 1.2	0.6 ± 0.2

Table 3: The yield strength determined by compression tesing parallel and perpendicular to the freezing direction and the peak stress in the parallel direction for the freeze-casted Cu-Ni foams.

Composition	Yield Strength [MPa]		Peak Stress [MPa]
	Parallel	Perpendicular	Parallel
Cu	39 ± 5	12 ± 2	56 ± 10
Cu_7Ni_3	41 ± 6	6 ± 1	72 ± 8
Cu_5Ni_5	57 ± 10	10 ± 2	87 ± 9
Cu_3Ni_7	43 ± 3	5 ± 1	62 ± 6
Ni	8 ± 2	4 ± 1	13 ± 3

Table 4: The energy absorbed at a strain of 0.4 during compression parallel and perpendicular to the freezing direction for the freeze-casted Cu-Ni foams.

Composition	Absorbed Energy [MJ/m^3]	
	Parallel	Perpendicular
Cu	15 ± 1	15 ± 2
Cu_7Ni_3	34 ± 3	30 ± 9
Cu_5Ni_5	31 ± 4	23 ± 2
Cu_3Ni_7	20 ± 2	12 ± 1
Ni	5 ± 1	6 ± 2

Table 5: The calculated equivalent yield strength of the struts for the freeze-casted Cu-Ni foams with a grain size of 1 μm.

Composition	Equivalent Yield Strength of the Struts [MPa]
Cu	205 ± 31
Cu_7Ni_3	252 ± 37
Cu_5Ni_5	364 ± 71
Cu_3Ni_7	319 ± 30
Ni	201 ± 54

Supplementary materials:

Video “Cu5Ni5_parallel.flv”: The deformation parallel to the freezing direction for the alloy Cu_5Ni_5.

Video “Cu5Ni5_perpendicular.flv”: The deformation perpendicular to the freezing direction for the alloy Cu_5Ni_5.